Pergamon

Int. J. Solids Structures Vol. 35, No. 33, pp. 4437–4456, 1998

0020–7683/98 $19.00 + .00

PII: S0020–7683(97)00241–2

ASPECTS OF NON-ASSOCIATED SINGLE CRYSTAL PLASTICITY: INFLUENCE OF NON-SCHMID EFFECTS AND LOCALIZATION ANALYSIS

P. STEINMANN*
Lehrstuhl für Technische Mechanik, Universität Kaiserslautern, D-67653 Kaiserslautern, Germany

E. KUHL
Institut für Baustatik, Universität Stuttgart, D-70550 Stuttgart, Germany

and

E. STEIN
Institut für Baumechanik und Numerische Mechanik, Universität Hannover, D-30167 Hannover, Germany

(*Received* 28 *February* 1997; *in revised form* 29 *July* 1997)

Abstract—The aim of this work is the consideration of so-called non-Schmid effects within non-associated single crystal plasticity at small strains. To this end, two additional activating mechanisms for dislocation flow on a slip system are modelled. For convenience the corresponding algorithmic setting is discussed in the sequel. Next, the influence of non-Schmid effects and non-associativity on the response behaviour of a single crystal within a simple shear deformation is examined. Subsequently, the theoretical framework for the localization analysis within multisurface plasticity is presented. Finally, the impact of non-Schmid effects on the orientation of a possible localization band and the corresponding critical hardening modulus are investigated for a simple model problem.

1. INTRODUCTION AND MOTIVATION

This contribution is concerned with different aspects of a single crystal plasticity formulation which takes into account additional non-Schmid effects at small strains.

Classically, the mathematical modelling of single crystal plasticity is associated with the Schmid yield condition which compares the critical shear stress on a crystallographic slip plane with the tangential projection of the global stress tensor. Thereby, the tangential stress projection, generally referred to as resolved Schmid stress, can be understood as the driving force activating the mechanism of dislocation flow. Motivated by the discrepancy between the Schmid based predictions and experimental results, a generalization of the Schmid law has been proposed, see e.g. the early contributions by Leroy *et al.* (1970) and Asaro and Rice (1977). Thereby, other stress projections than the Schmid stress are taken into account for the mobilization of dislocation flow.

In the present contribution we will focus on two essential non-Schmid stresses acting as additional driving forces for dislocation flow. On the one hand, we consider the projection onto the slip plane normal, i.e. the normal stress on the slip plane, and on the other hand we take the projection onto the co-slip direction, i.e. the co-shear stress on the slip plane, into account. In view of the crystallographic geometry, both non-Schmid stresses can be motivated as additional driving forces activating dislocation flow by either obstacle jumping or obstacle surrounding.

The underlying geometric interpretation of non-Schmid effects is based on several experimental observations for different crystalline materials. Christian (1983) gave an

* Author to whom correspondence should be addressed. Universitat Kaiserslautern, Lehrstuhl für Technische Mechanik, Postfach 3049, D-67653 Kaiserslautern, Germany.

exposition on "some surprising features of plastic deformation of bcc metal and alloys" which include besides other anomalous phenomena in particular the failure of the classical Schmid law. This anomal behaviour has as well been observed for intermetallic compounds of the so-called $L1_2$ structure based on an fcc lattice. Paidar *et al.* (1984) proposed a theory that explains the anomalous yield behaviour in $L1_2$ structures which appear to strongly disobey the Schmid law. Experimental investigations on Ni_3Ga and Co_3Ti have been performed by Ezz *et al.* (1992) and Takasugi *et al.* (1987) which again suggest that, due to the complex core structure of dislocations in the crystal, other stress components than the Schmid stress affect the mobility of dislocations on a slip plane.

These additional effects, sometimes resulting in cross-slip, where early modelled by Leroy *et al.* (1970) by reducing the yield stress. This formulation does not affect the driving force, which has been modelled to be identical to the one predicted by the Schmid law. Although this seems to be a different motivation, the results obtained by Leroy *et al.* (1970) coincide with a formulation where non-Schmid stresses are considered as being responsible for the activation of the slip mechanism. A phenomenological framework within a continuum description was proposed by Asaro and Rice (1977) and Asaro (1983) who also analysed the effects on the localization analysis if non-Schmid contributions are considered. An overall account on single crystal plasticity including non-Schmid effects is given by Qin and Bassani (1992a, b) and Bassani (1994) with particular emphasis on aspects related to the underlying non-associated plasticity formulation. Non-normality, which is for example introduced through the additional consideration of normal stress components in the yield condition, leads to destabilizing effects, thus even for positive hardening moduli the tendency towards the formation of localization bands can be predicted, which essentially coincides with experimental results. Moreover, the orientation of the localization band and the active slip planes do not agree, but obey a slight mismatch, see Chang and Asaro (1981) and Spitzig (1981).

The paper is organized as follows: first, in order to embed the basic equations of single crystal plasticity at small strains into the framework of phenomenological continuum mechanics, we review the essential relations of multisurface elasto-plasticity. Thereby, for the phenomenological modelling within a continuum mechanics setting, it is widely accepted that models of single crystal plasticity may be considered as particular examples of multisurface plasticity, see for example the early contributions by Koiter (1960) and Mandel (1972).

Next we give a brief description of a generalized single crystal plasticity model taking into account additional non-Schmid effects. Thereby, the well-accepted formulation based on the Schmid law is enriched by two additional stress components, the normal stress and the co-shear stress acting on the slip plane. The traditional framework for single crystal plasticity is set forth e.g. in Hill (1966), Hill and Havner (1982), Asaro (1983) among others. As a simplification the constitutive equations for non-Schmid crystal plasticity are specialized for a prototype model problem assuming isotropic elastic behaviour and plasticity based on the isotropic flow resistance.

As far as the algorithmic implementation is concerned, recent computational treatments of Schmid based single crystal plasticity have been advocated e.g. by Cuitiño and Ortiz (1992), Borja and Wren (1993), Steinmann and Stein (1996), Miehe (1996) and Anand and Kothari (1996). After reviewing the algorithmic treatment of the non-Schmid version of single crystal plasticity and discussing the main differences to single surface plasticity, we examine the influence of the additional non-Schmid effects in a model example in form of a simple shear test.

In the second part of this work, we are concerned with the localization analysis of the proposed single crystal model. To this end, we first derive the localization condition for two different scenarios which are commonly denoted as continuous and discontinuous localization. Thereby, the possibility for several active slip systems is taken into account and results in explicit formulations for the critical hardening modulus. Finally, we investigate the critical hardening modulus and the corresponding direction of a possible localization band for a simple model problem whereby we focus in particular on the effects of the non-associated flow rule which is due to the consideration of the additional non-Schmid contributions.

2. SINGLE CRYSTAL PLASTICITY AT SMALL STRAINS

2.1. *Multisurface plasticity framework*

To set the stage of the subsequent developments, we first review the essential relations of geometrically linear multisurface elasto-plasticity.

Classically, the underlying kinematical assumption is the additive decomposition of the total strain into an elastic and a plastic part

$$\boldsymbol{\varepsilon} = \boldsymbol{\varepsilon}_e + \boldsymbol{\varepsilon}_p \quad \text{with } \boldsymbol{\varepsilon} = \nabla_x^{\text{sym}} \mathbf{u} \quad \text{and} \quad \mathbf{u} \in \mathbb{R}^n_{\text{dim}}. \tag{1}$$

Then, the elastic part of the constitutive law is formulated via the fourth order elastic tangent operator $\mathscr{E}_{el}$, not necessarily isotropic, of the geometrically linear theory and, moreover, n_{srf} yield stresses Y_I are introduced in terms of n_{srf} scalar internal variables κ_J which are responsible for isotropic hardening

$$\boldsymbol{\sigma} = \mathscr{E}_{el} : \boldsymbol{\varepsilon}_e \quad \text{and} \quad Y_I = Y_I(\kappa_J) \quad \forall I, J = 1 \ldots n_{srf}. \tag{2}$$

The structure of the dissipation inequality suggests n_{srf} yield conditions Φ_I in terms of the stress measure $\boldsymbol{\sigma}$ and the yield stress Y_I

$$\Phi_I(\boldsymbol{\sigma}, Y_I) = \varphi_I(\boldsymbol{\sigma}) - Y_I \leqslant 0 \quad \text{with } \mathbf{v}_I = \frac{\partial \varphi_I}{\partial \boldsymbol{\sigma}} \quad \forall I = 1 \ldots n_{srf}. \tag{3}$$

Here, the $\mathbf{v}_I$ denote the normals to the yield conditions in the stress space. Moreover, for the general non-associated case a Koiter type flow rule in terms of the flow directions $\boldsymbol{\mu}_I$ together with the evolution equations for the internal variables κ_I are given by

$$\dot{\boldsymbol{\varepsilon}}_p = \sum_{I=1}^{n_{srf}} \gamma_I \boldsymbol{\mu}_I \quad \text{and} \quad \dot{\kappa}_I = \gamma_I \quad \forall I = 1 \ldots n_{srf}. \tag{4}$$

Accordingly, the evolution of the yield stresses Y_I renders the hardening moduli H_{IJ}

$$\dot{Y}_I = \sum_{J=1}^{n_{srf}} H_{IJ} \gamma_J \quad \text{with } H_{IJ} = \frac{\partial Y_I}{\partial \kappa_J}. \tag{5}$$

Plastic-loading and elastic-unloading conditions together with the requirement of consistency are expressed for each yield condition as

$$\gamma_I \geqslant 0 \quad \Phi_I(\boldsymbol{\sigma}, Y_I) \leqslant 0 \quad \gamma_I \Phi_I(\boldsymbol{\sigma}, Y_I) = 0 \quad \text{and} \quad \gamma_I \dot{\Phi}_I(\boldsymbol{\sigma}, Y_I) = 0. \tag{6}$$

The special case of associated plasticity is obtained upon substituting $\boldsymbol{\mu}_I$ by $\mathbf{v}_I$ whereby the principle of maximum dissipation will be satisfied. For associated plasticity the loading–unloading conditions follow from the optimality conditions that are implied by the principle of maximum dissipation. In terms of an optimization problem with n_{srf} inequality constraints they represent the classical Kuhn–Tucker complementary conditions. For non-associated plasticity they are rather postulated by physical reasoning. Since generally not all n_{srf} yield conditions are simultaneously active, we define in addition the set of active constraints $\mathscr{A}$, whereby we assume for simplicity that all active constraints are independent

$$\mathscr{A} = \{I \in \{1 \ldots n_{srf}\} \,|\, \Phi_I = 0 \text{ and } \gamma_I > 0\} \quad \text{with } n_{act} = \dim \mathscr{A}. \tag{7}$$

Evaluating the consistency conditions for the Φ_I in eqn (6.4) for the case of plastic loading yields after some algebraic manipulations the plastic multipliers γ_I in two alternative expressions.

$$\gamma_I = \tilde{\mathbf{v}}_I : \mathbb{E}_{el} : \dot{\boldsymbol{\varepsilon}} > 0 \quad \text{or} \quad \gamma_I = \bar{\mathbf{v}}_I : \dot{\boldsymbol{\sigma}} > 0 \quad \forall I \in \mathscr{A}. \tag{8}$$

Thereby, the latter expression is valid as long as the matrix of hardening moduli H_{IJ} is not singular. In the above relations we introduced the pseudo surface normals $\tilde{\mathbf{v}}_I$ and $\bar{\mathbf{v}}_I$ as convenient abbreviations

$$\tilde{\mathbf{v}}_I = \sum_{J \in \mathscr{A}} h^{IJ} \mathbf{v}_J \quad \text{and} \quad \bar{\mathbf{v}} = \sum_{J \in \mathscr{A}} H^{IJ} \mathbf{v}_J \quad \forall I \in \mathscr{A}. \tag{9}$$

with $[h^{IJ}] = [h_{IJ}]^{-1}$ and $[H^{IJ}] = [H_{IJ}]^{-1}$.

Finally, the coefficients h_{IJ} are defined in terms of the hardening moduli H_{IJ} and the coefficients η_{IJ}

$$h_{IJ} = \eta_{IJ} + H_{IJ} \quad \text{and} \quad \eta_{IJ} = \mathbf{v}_I : \mathbb{E}_{el} : \boldsymbol{\mu}_J. \tag{10}$$

As a result we obtain the elasto-plastic tangent operator and its inverse in the remarkably simple format of a sum of rank one updates

$$\mathbb{E}_{ep} = \mathbb{E}_{el} - \sum_{I \in \mathscr{A}} \mathbb{E}_{el} : \boldsymbol{\mu}_I \otimes \tilde{\mathbf{v}}_I : \mathbb{E}_{el} \quad \text{and} \quad \mathbb{E}_{ep}^{-1} = \mathbb{E}_{el}^{-1} + \sum_{I \in \mathscr{A}} \boldsymbol{\mu}_I \otimes \bar{\mathbf{v}}_I. \tag{11}$$

Please observe that the tangent operator is non-symmetric for the general non-associated case.

2.2. *Application to single crystal plasticity*

At the micro level the geometry of a single crystal lattice is essentially characterized by the planes with maximum density of atoms, the so-called slip planes with normal unit vector $\mathbf{m}_I$, and the directions with minimum distance between the atoms, typically in the order of 1 Å, the so-called slip directions $\mathbf{s}_I$, see Fig. 1. For ductile single crystals these vectors possess the property $\mathbf{s}_I \perp \mathbf{m}_I$ for each crystallographic slip system I. Therefore, it appears meaningful to complement these vectors to an orthogonal triad by the so-called co-slip direction $\mathbf{c}_I = \mathbf{s}_I \times \mathbf{m}_I$. Then we introduce the following dyadics for later use

$$\mathbf{s}_I \otimes \mathbf{m}_I \quad \text{and} \quad \mathbf{m}_I \otimes \mathbf{m}_I \quad \text{and} \quad \mathbf{c}_I \otimes \mathbf{m}_I. \tag{12}$$

These dyadics are used to project the stress tensor $\boldsymbol{\sigma}$ onto certain stress components acting on the slip plane I. We will denote these components by τ_I^{sm}, τ_I^{mm} and τ_I^{cm}, they are defined as

$$\tau_I^{sm} = \boldsymbol{\sigma} : [\mathbf{s}_I \otimes \mathbf{m}_I] \quad \text{and} \quad \tau_I^{mm} = \boldsymbol{\sigma} : [\mathbf{m}_I \otimes \mathbf{m}_I] \quad \text{and} \quad \tau_I^{cm} = \boldsymbol{\sigma} : [\mathbf{c}_I \otimes \mathbf{m}_I]. \tag{13}$$

In particular, the so-called Schmid tensor $\mathbf{s}_I \otimes \mathbf{m}_I$ projects the stress tensor $\boldsymbol{\sigma}$ onto the shear

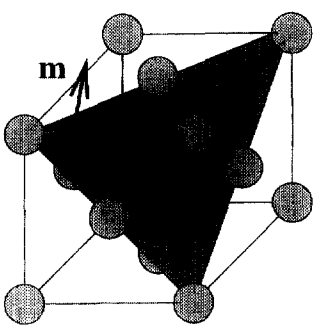

Fig. 1. Characteristic directions **s**, **c** and **m**.

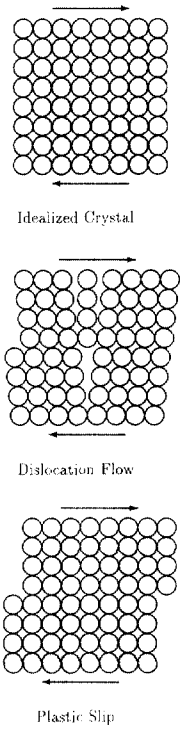

Fig. 2. Mechanism of plastic slip.

stress τ_I^{sm}, frequently referred to as the resolved Schmid stress, which acts in the direction $\mathbf{s}_I$ of the slip plane I. Accordingly, the non-Schmid tensors $\mathbf{m}_I \otimes \mathbf{m}_I$ and $\mathbf{c}_I \otimes \mathbf{m}_I$ project $\boldsymbol{\sigma}$ into the normal stress τ_I^{mm} and the co-shear stress τ_I^{cm}, commonly referred to as non-Schmid stresses, acting on the slip plane I.

For single crystals irreversible deformations are accumulated by the flow of single dislocations through the crystal lattice, for a sketch of the mechanism of dislocation flow please refer to Fig. 2. Within a continuum theory the flow of single dislocations is homogenized into the notion of plastic slip.

In general, all components τ_I^{sm}, τ_I^{mm} and τ_I^{cm}, weighted by corresponding influence values α^{sm}, α^{mm}, α^{cm} might be responsible for the activation of plastic slip in slip system I, thus, on each slip system I plastic slip occurs as soon as a critical reference value, the flow resistance Y_I, is exceeded

$$\Phi_I = \varphi_I(\boldsymbol{\sigma}) - Y_I = \alpha^{sm}\tau_I^{sm} + \alpha^{mm}\tau_I^{mm} + \alpha^{cm}\tau_I^{cm} - Y_I \leqslant 0. \tag{14}$$

The arrest and pile up of single dislocations together with other point effects like vacancies and interstitial atoms render an obstacle for the dislocation flow and thus, leads to an increased flow resistance Y_I. These hardening effects are phenomenologically measured by the internal variables κ_I.

It is interesting to note that the yield condition, a linear and homogeneous function of degree one in the stress, might be simplified into the notation of the previous section as

$$\varphi_I = \boldsymbol{\sigma} : \frac{\partial \phi_I}{\partial \boldsymbol{\sigma}} = \boldsymbol{\sigma} : \boldsymbol{v}_I \quad \text{with } \boldsymbol{v}_I = \alpha^{sm}[\mathbf{s}_I \otimes \mathbf{m}_I]^{sym} + \alpha^{mm}[\mathbf{m}_I \otimes \mathbf{m}_I] + \alpha^{cm}[\mathbf{c}_I \otimes \mathbf{m}_I]^{sym}. \tag{15}$$

The classical Schmid based formulation is obtained by setting $\alpha^{sm} = 1$ and $\alpha^{mm} = \alpha^{cm} = 0$ giving Y_I the interpretation of the critical resolved shear stress on slip system I. The non-Schmid contributions due to $\alpha^{mm} \neq 0$ and $\alpha^{cm} \neq 0$, i.e. due to the normal stress and the co-shear stress on the slip plane, take additional activating mechanisms (obstacle jumping and

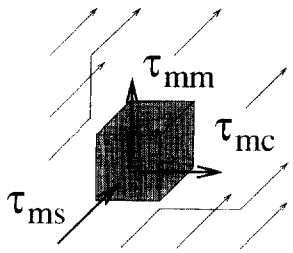

Fig. 3. Activating mechanisms for plastic slip.

obstacle surrounding) for dislocation flow into account, as a motivation consider Fig. 3. Thereby, in order to account for the additional activating mechanisms irrespectively of the sign of the normal stress and the co-shear stress we assume for the influence values α^{mm}, α^{cm}

$$\text{sign}(\alpha^{mm}) = \text{sign}(\tau_I^{mm}) \quad \text{and} \quad \text{sign}(\alpha^{cm}) = \text{sign}(\tau_I^{cm}). \tag{16}$$

From the geometry of a crystal lattice the evolution law for the plastic strains or rather the flow rule turns out to be dictated by the flow of dislocations along fixed slip systems in the so-called isoclinic configuration even if non-Schmid effects are present

$$\dot{\boldsymbol{\varepsilon}}_p = \sum_{I \in \mathcal{I}} \gamma_I [\mathbf{s}_I \otimes \mathbf{m}_I]^{sym}. \tag{17}$$

Here the plastic multipliers γ_I take the interpretation as the rates of plastic slip on the slip systems I. Please note that plastic flow is assumed to preserve the plastic volume since we have simple shear with $\mathbf{s}_I \perp \mathbf{m}_I$ for each crystallographic slip system I thus, rendering $\dot{\boldsymbol{\varepsilon}}_p : \mathbf{I} = 0$. The flow rule might be simplified into the notation of the previous section as

$$\dot{\boldsymbol{\varepsilon}}_p = \sum_{I \in \mathcal{I}} \gamma_I \boldsymbol{\mu}_I \quad \text{with } \boldsymbol{\mu}_I = [\mathbf{s}_I \otimes \mathbf{m}_I]^{sym} \neq \boldsymbol{\nu}_I. \tag{18}$$

Typically, for fcc crystals 24 (counting slip in positive and negative slip direction separately) slip systems might be activated in a general deformation. These are given by combinations of the four $\mathbf{m}_I \in \{111\}$ planes and the three $\mathbf{s}_I \in [110]$ directions of a crystal unit cell, see Fig. 4.

As a summary of this section, single crystal plasticity might be considered as the paradigm for multisurface plasticity with anisotropic yield conditions. Thereby, on the one hand, Schmid based single crystal plasticity in the format advocated e.g. by Asaro (1983) falls into the category of associated multisurface plasticity, whereas, on the other hand, non-Schmid based single crystal plasticity in the format advocated e.g. by Bassani (1994) falls into the category of non-associated multisurface plasticity.

2.3. *Prototype model problem*

For the sake of simplicity we restrict ourselves to the geometrically linear case and assume the elastic response to be governed by the isotropic Hooke model valid for small strains

$$\mathcal{E}_{el} = 2G\mathcal{I}^{dev} + K\mathbf{I} \otimes \mathbf{I} \quad \text{with } \mathcal{I}^{dev} = \mathcal{I} - \tfrac{1}{3}\mathbf{I} \otimes \mathbf{I}. \tag{19}$$

Here G and K are the shear and bulk modulus, respectively, $\mathcal{I}$ and $\mathbf{I}$ denote the fourth and second order unit tensors. The elastic stress response decouples into the deviatoric stress $\mathbf{s}$ and the hydrostatic pressure p as

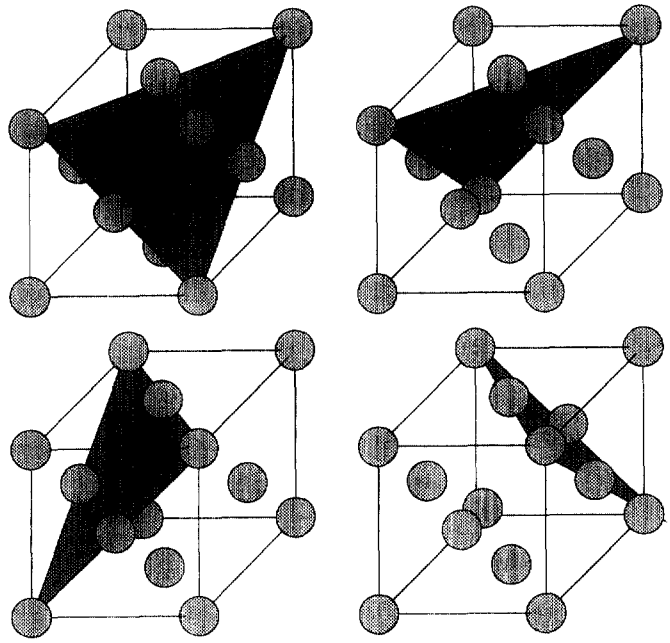

Fig. 4. Slip systems of an FCC crystal.

$$\boldsymbol{\sigma} = \mathbf{s} + p\mathbf{I} \quad \text{with } \mathbf{s} = 2G\mathscr{I}^{dev} : \boldsymbol{\varepsilon}_e \quad \text{and} \quad p = K\mathbf{I} : \boldsymbol{\varepsilon}_e. \tag{20}$$

Then the projected stress components τ_I^{sm}, τ_I^{nnm}, τ_I^{cm} are computed almost exclusively in terms of the deviatoric stress $\mathbf{s}$

$$\tau_I^{sm} = \mathbf{s} : [\mathbf{s}_I \otimes \mathbf{m}_I] \quad \text{and} \quad \tau_I^{nnm} = \mathbf{s} : [\mathbf{m}_I \otimes \mathbf{m}_I] + p \quad \text{and} \quad \tau_I^{cm} = \mathbf{s} : [\mathbf{c}_I \otimes \mathbf{m}_I]. \tag{21}$$

Apparently, only τ_I^{nnm} renders a dependence of the hydrostatic pressure p which is usually neglected in the plasticity formulation for ductile single crystals. The projection of the flow direction $\boldsymbol{\mu}_I$ and the yield surface normals $\boldsymbol{\nu}_J$ by the elastic tangent operator simplifies into

$$\mathscr{E}_{el} : \boldsymbol{\mu}_I = 2G\boldsymbol{\mu}_I \quad \text{and} \quad \boldsymbol{\nu}_J : \mathscr{E}_{el} = 2G\boldsymbol{\nu}_J^{dev} + \alpha^{nnm} K\mathbf{I} \quad \text{with } \boldsymbol{\nu}_J^{dev} = \boldsymbol{\nu}_J - \tfrac{1}{3}\alpha^{nnm}\mathbf{I}. \tag{22}$$

A further simplification is obtained by assuming an isotropic flow resistance $Y_I = Y$ for all slip systems I and lateral Taylor hardening $H_{IJ} = H$ in terms of a single internal variable κ with evolution law

$$\dot{\kappa} = \sum_{I \in \mathscr{A}} \gamma_I \quad \text{and} \quad \dot{Y} = H\dot{\kappa} \quad \text{where} \quad Y = Y(\kappa) \quad \text{and} \quad H = \frac{\partial Y}{\partial \kappa}. \tag{23}$$

Typically, for Al–Cu alloys the saturation type critical flow resistance Y and its derivative, the hardening modulus H, might be assumed as

$$Y(\kappa) = Y_0 + [Y_\infty - Y_0] \tanh\left(\frac{H_0\kappa}{Y_\infty - Y_0}\right) \quad \text{and} \quad H(\kappa) = H_0 \cosh^{-2}\left(\frac{H_0\kappa}{Y_\infty - Y_0}\right) \tag{24}$$

with Y_0, Y_∞ and H_0 the initial flow resistance, the saturation flow resistance and the initial hardening rate, respectively.

Based on the above assumptions the non-symmetric tangent operator is explicitly expanded as

Table 1. Prototype non-Schmid single crystal plasticity

- Elastic constitutive law

$$\mathbf{s} = 2G\mathbb{I}^{dev} : [\boldsymbol{\varepsilon} - \boldsymbol{\varepsilon}_p] \text{ and } p = K\mathbf{I} : [\boldsymbol{\varepsilon} - \boldsymbol{\varepsilon}_p]$$

- Projected stresses

$$\tau_I^{sym} = \mathbf{s} : [\mathbf{s}_I \otimes \mathbf{m}_I] \quad \tau_I^{mm} = \mathbf{s} : [\mathbf{m}_I \otimes \mathbf{m}_I] + p \quad \tau_I^{cm} = \mathbf{s} : [\mathbf{c}_I \otimes \mathbf{m}_I]$$

- Yield conditions

$$\Phi_I = \varphi_I - Y \leqslant 0 \quad \text{with} \quad \varphi_I = \alpha^{sm}\tau_I^{sm} + \alpha^{mm}\tau_I^{mm} + \alpha^{cm}\tau_I^{cm}$$

- Flow resistance

$$Y(\kappa) = Y_0 + [Y_\infty - Y_0] \tanh\left(\frac{H_0 \kappa}{Y_\infty - Y_0}\right)$$

- Flow rule and evolution law for the hardening variable

$$\dot{\boldsymbol{\varepsilon}}_p = \sum_{I \in \mathscr{A}} \dot{\gamma}_I \boldsymbol{\mu}_I \quad \text{and} \quad \dot{\kappa} = \sum_{I \in \mathscr{A}} \dot{\gamma}_I$$

- Elasto-plastic tangent operator

$$\mathbb{C}_{ep} = \mathbb{C}_{el} - \sum_{I,J \in \mathscr{A}} h^{IJ} [2G\boldsymbol{\mu}_I] \otimes [2G\mathbf{v}_J^{dev} + \alpha^{mm} K\mathbf{I}]$$

$$\mathbb{C}_{ep} = \mathbb{C}_{el} - \sum_{I,J \in \mathscr{A}} h^{IJ} [2G\boldsymbol{\mu}_I] \otimes [2G\mathbf{v}_J^{dev} + \alpha^{mm} K\mathbf{I}] \quad \text{with } h_{IJ} = 2G\mathbf{v}_I : \boldsymbol{\mu}_J + H. \tag{25}$$

For convenience, the resulting single crystal model is summarized in Table 1.

3. ALGORITHMIC TREATMENT

Following standard procedure in computational elasto-plasticity, the flow rule and the evolution law for the hardening variable are integrated over a finite time step $\Delta t = {}^{n+1}t - {}^{n}t$ by the Euler backward method to obtain

$$\Delta\boldsymbol{\varepsilon}_p = \sum_{I \in \mathscr{A}} \Delta\gamma_I \boldsymbol{\mu}_I \quad \text{and} \quad \Delta\kappa = \sum_{I \in \mathscr{A}} \Delta\gamma_I \quad \text{with } \Delta\gamma_I = \Delta t \dot{\gamma}_I. \tag{26}$$

Assuming first that the response during Δt is purely reversible, i.e. the active set of slip systems is empty $\mathscr{A} = \varnothing$, the elastic predictor state is given by

$${}^{e}\boldsymbol{\sigma} = \mathbb{C}_{el} : [{}^{n+1}\boldsymbol{\varepsilon} - {}^{n}\boldsymbol{\varepsilon}_p] \quad {}^{e}\varphi_I = {}^{e}\boldsymbol{\sigma} : \mathbf{v}_I \quad {}^{e}\kappa = {}^{n}\kappa \rightsquigarrow {}^{e}\Phi_I = {}^{e}\varphi_I - Y({}^{e}\kappa). \tag{27}$$

The violation of any of the yield conditions ${}^{e}\Phi_I > 0$ by the elastic predictor state determines if a plastic corrector step must be performed.

Thereby, the determination of the active slip systems or rather the set of active constraints $\mathscr{A}$, poses severe difficulties. On the one hand, due to the incompressibility constraint for the plastic flow, a maximum number of five independent slip systems is possible within $3d$ multisurface elasto-plasticity. On the other hand, for the case of fcc single crystals, 24 slip systems might be activated, thus, the determination of the active slip systems in non-unique. For the selection of the active set of slip systems a number of proposals has been made recently, see e.g. Simo *et al.* (1988) for the case of linearly independent constraints and Cuitiño and Ortiz (1992), Borja and Wren (1993), Anand and Kothari (1996) for the case of linearly dependent constraints.

In the sequel, we apply the algorithm proposed by Cuitiño and Ortiz (1992) which basically adds the most loaded system to the set of active constraints in an iterative fashion. Numerical experience proves that this algorithm renders a converging sequence of Newton

iterations. When the active set of slip systems is determined, the incremental slip rates $\Delta\gamma_I$ follow from the solution of the implicit algorithmic consistency condition

$$^{n+1}\Phi_I = {}^{c}\varphi_I - \sum_{J\in\mathcal{A}} \Delta\gamma_J \eta_{IJ} - Y\left({}^{c}\kappa + \sum_{J\in\mathcal{A}} \Delta\gamma_J\right) \doteq 0. \tag{28}$$

Thereby, a typical iterative Newton update is given in combination with a Bertsekas projection by

$$\Delta\gamma_I = \max\left\{\left(\Delta\gamma_I + \sum_{J\in\mathcal{A}} h^{IJ\,n-1}\Phi_J\right), 0\right\}. \tag{29}$$

The coefficients η_{IJ} are expressed in terms of the slip and co-slip directions $\mathbf{s}_I$ and $\mathbf{c}_I$ together with the slip plane normal $\mathbf{m}_I$. Since these are fixed in the isoclinic configuration, they might be computed in advance from the scalar products

$$\eta_{IJ} = G[\alpha^{sm}[\mathbf{s}_I\cdot\mathbf{s}_J] + \alpha^{cm}[\mathbf{c}_I\cdot\mathbf{s}_J] + \alpha^{mm}[\mathbf{m}_I\cdot\mathbf{s}_J]][\mathbf{m}_I\cdot\mathbf{m}_J] \tag{30}$$

$$+ G[\alpha^{sm}[\mathbf{s}_I\cdot\mathbf{m}_J] + \alpha^{cm}[\mathbf{c}_I\cdot\mathbf{m}_J] + \alpha^{mm}[\mathbf{m}_I\cdot\mathbf{m}_J]][\mathbf{m}_I\cdot\mathbf{s}_J]. \tag{31}$$

In summary, the update of the stress and the internal variable is given in the following form

$$^{n+1}\boldsymbol{\sigma} = {}^{c}\boldsymbol{\sigma} - 2G\sum_{I\in\mathcal{A}} \Delta\gamma_I \boldsymbol{\mu}_I \quad \text{and} \quad {}^{n+1}\kappa = {}^{c}\kappa + \sum_{I\in\mathcal{A}} \Delta\gamma_I. \tag{32}$$

Finally, the algorithmic elasto-plastic tangent operator $\mathscr{E}^{a}_{ep}$, necessary to guarantee optimal quadratic convergence within the global Newton–Raphson equilibrium iteration, is obtained by linearizing the stress update algorithm $^{n+1}\boldsymbol{\sigma}({}^{c}\boldsymbol{\varepsilon})$. In the sequel we will employ this tangent operator exclusively within the localization analysis. Remarkably, for the present case of single crystal plasticity the algorithmic tangent operator is identical to the continuum elasto-plastic tangent operator, thereby this coincidence is due to the linearity of the yield conditions in the stresses

$$\mathrm{d}\boldsymbol{\sigma} = \mathscr{E}^{a}_{ep} : \mathrm{d}\boldsymbol{\varepsilon} \rightsquigarrow \mathscr{E}^{a}_{ep} \equiv \mathscr{E}_{ep}. \tag{33}$$

Recall that in contrast to Schmid based single crystal plasticity, non-Schmid based single crystal plasticity obeys a non-associated flow rule. As a consequence, the corresponding tangent operator and thus the overall linearized system of equations resulting from a finite element discretization are non-symmetric. Within a computational setting non-symmetric systems of equations lead to a slightly increased amount of work spent for the solver.

The resulting algorithmic counterpart of the present single crystal model is summarized for convenience in Table 2.

4. EXAMPLE: PLANAR SIMPLE SHEAR DEFORMATION

In this example of phenomenological influence of non-Schmid effects on the response behaviour of a single crystal undergoing a homogeneous simple shear deformation under plane strain conditions is examined numerically.

The material parameters are chosen to model an Al–Cu alloy with Lamé constants $L = 35{,}105$ N/mm^2 and $G = 23{,}427$ N/mm^2. The initial flow resistance, the saturation flow resistance and the initial hardening rate are set to $Y_0 = 60.5$ N/mm^2, $Y_\infty = 109.5$ N/mm^2 and $H_0 = 541.5$ N/mm^2, respectively. For the kinematics of the crystal we restrict ourselves for simplicity to the Asaro planar double slip model, thus the non-Schmid effects exclusively

Table 2. Integration algorithm for Schmid and non-Schmid single crystal plasticity

1. Increment initialization $\eta_{IJ} = 2G\boldsymbol{v}_I : \boldsymbol{\mu}_J$, $\mathscr{A} = \varnothing$ and predictor state

$$^{e}\boldsymbol{\sigma} = \mathscr{E}_{el} : [^{n+1}\boldsymbol{\varepsilon} - {}^{n}\boldsymbol{\varepsilon}_p] \quad ^{e}\varphi_I = {}^{e}\boldsymbol{\sigma} : \boldsymbol{v}_I \quad ^{e}\kappa = {}^{n}\kappa \quad ^{e}\Phi_I = {}^{e}\varphi_I - Y(^{e}\kappa)$$

2. Iteration initialisation

$$^{n+1}\Phi_I = {}^{e}\Phi_I, \quad ^{n+1}\kappa = {}^{e}\kappa \text{ and } \Delta\gamma_I = 0$$

3. Newton step with iteration matrix $h_{IJ} + H(^{n+1}\kappa)$, projection and filter

$$\Delta\gamma_I = \max\left\{\left(\Delta\gamma_I + \sum_{J\in\mathscr{A}} h^{IJ\,n+1}\Phi_J\right), 0\right\} \quad \mathscr{A} = \mathscr{A} \cup I(\Delta\gamma_I = 0)$$

4. Iteration update

$$^{n+1}\varphi_I = {}^{e}\varphi_I - \sum_{J\in\mathscr{A}} \Delta\gamma_J \eta_{IJ} \quad ^{n+1}\kappa = {}^{n}\kappa + \sum_{I\in\mathscr{A}} \Delta\gamma_I \quad ^{n+1}\Phi_I = {}^{n+1}\varphi_I - Y(^{n+1}\kappa)$$

5. Check residuum for active slip systems

$$\text{If } \sum_{I\in\mathscr{A}} |^{n+1}\Phi_I|^2 \geqslant \text{Tol}^2 \text{ then Goto 3}$$

6. Check residuum for all slip systems

$$\text{If } \sum_{I=1}^{n_{sl}} \langle ^{n+1}\Phi_I\rangle^2 \geqslant \text{Tol}^2 \text{ then } \mathscr{A} = \mathscr{A} \bigcup I(\max {}^{n+1}\Phi_I) \text{ and Goto 2}$$

7. Increment update

$$^{n+1}\boldsymbol{\sigma} = {}^{e}\boldsymbol{\sigma} - 2G \sum_{I\in\mathscr{A}} \Delta\gamma_I \boldsymbol{\mu}_I, \quad ^{n+1}\kappa = {}^{e}\kappa + \sum_{I\in\mathscr{A}} \Delta\gamma_I$$

8. Algorithmic elasto-plastic tangent operator

$$\mathscr{E}^{a}_{ep} = \mathscr{E}_{el} - \sum_{I,J\in\mathscr{A}} h^{IJ}[2G\boldsymbol{\mu}_I] \otimes [2G\boldsymbol{v}_J^{dev} + \alpha^{mm}\boldsymbol{K}\mathbf{I}]$$

stem from the normal stress τ_I^{mm} and the influence value α^{mm}. The two-slip planes are symmetrically oriented with $\pm 30^\circ$ about the global $\mathbf{e}_2$ direction.

The analysis is performed displacement driven for a single integration point of a standard **Q**1 element. Thereby, the shear strain is applied in 50 prescribed deformation steps with $\Delta\varepsilon_{12} = 0.1\%$ until a final value of $\varepsilon_{12} = 5.0\%$ is obtained.

The effects of the non-Schmid contribution are examined by increasing the influence value α^{mm} from $\alpha^{mm} = 0\%$, representing the special case of the underlying Schmid behaviour, to $\alpha^{mm} = 20\%$, representing strong additional non-Schmid activating mechanisms for plastic slip. Thereby, we focus primarily on the resulting shear stress component σ_{12} with respect to the fixed Cartesian laboratory frame. Moreover, the evolution of the flow resistance Y and the internal variable κ are observed.

Figure 5 reflects the evolution of the shear stress component σ_{12} for varying influence values α^{mm}. When the elastic regime is left the resulting shear stress decreases with increasing values of α^{mm} in the plastic regime. For the interpretation of these results we recall that the flow resistance Y coincides with the projected stress φ_I on the active slip systems I. Thereby, it turns out that the order of magnitude for the flow resistance Y displayed over the shear strain ε_{12} in Fig. 7 is almost independent of the chosen α^{mm}. The projected stress φ_I is in turn computed by projecting the stress tensor $\boldsymbol{\sigma}$ by the projection tensor $\boldsymbol{v}_I$, whereby the influence of τ_I^{mm} is emphasized with increasing α^{mm}. Therefore, the load carrying capacity of the material in Fig. 5 decreases with increasing non-Schmid contributions. For the particular model of non-Schmid single crystal plasticity under consideration this behaviour seems to characterize a general trend.

For the sake of comparison Fig. 6 displays the difference of the associated and the non-associated version of the flow rule for $\alpha^{mm} = 20\%$ and contrasts the results to the standard Schmid rule with $\alpha^{mm} = 0\%$. On the one hand, the load carrying capacity obviously decreases as soon as any non-Schmid contributions are taken into account. On the other

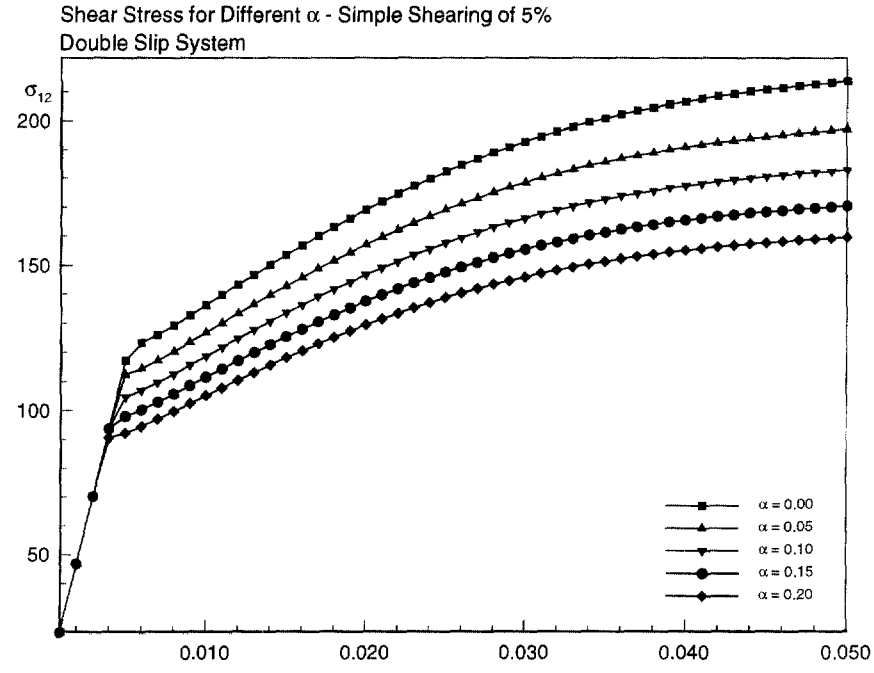

Fig. 5. Shear stresses for different α^{mn}.

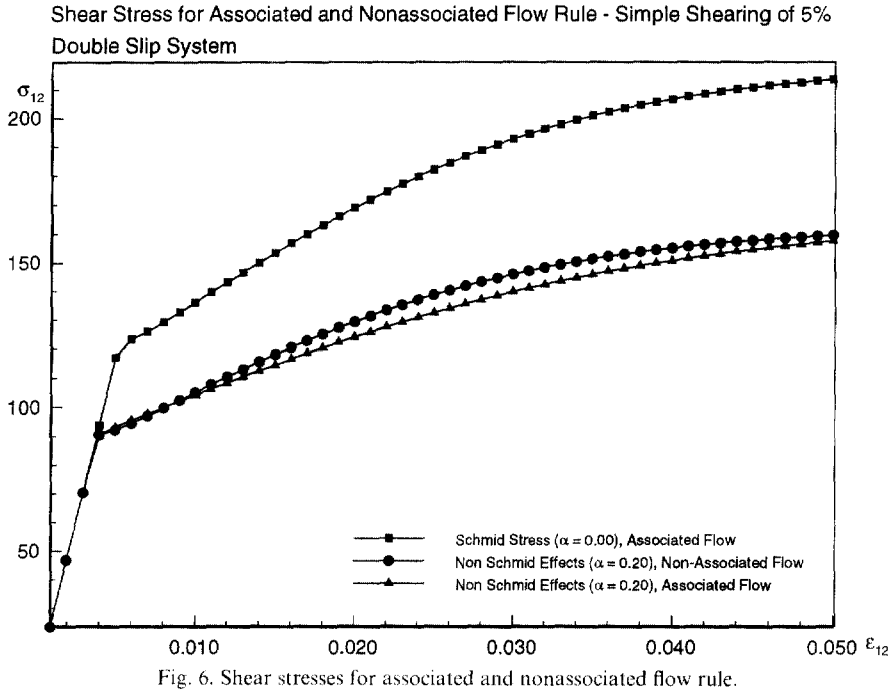

Fig. 6. Shear stresses for associated and nonassociated flow rule.

hand, there is only a slight difference in the response for the associated and the non-associated case. Thereby, the stress–strain curve of the non-associated flow rule takes slightly higher values as compared to the corresponding curve of the associated flow rule. Nevertheless, as soon as the flow resistance is saturated this distinction vanishes.

The influence of α^{mn} on the evolution of the internal variable κ and the resulting flow resistance Y is highlighted in Figs 7 and 8. The resulting curves indicate a moderate increase of the obstacle density with increasing α^{mn}. therefore the saturated flow resistance is achieved

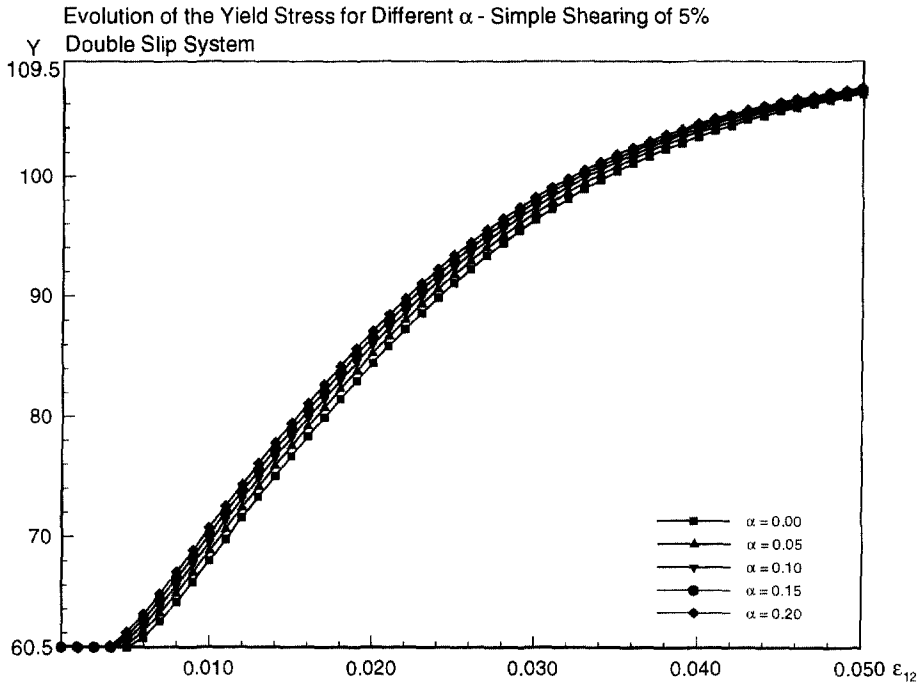

Fig. 7. Yield stress for different α^{min}.

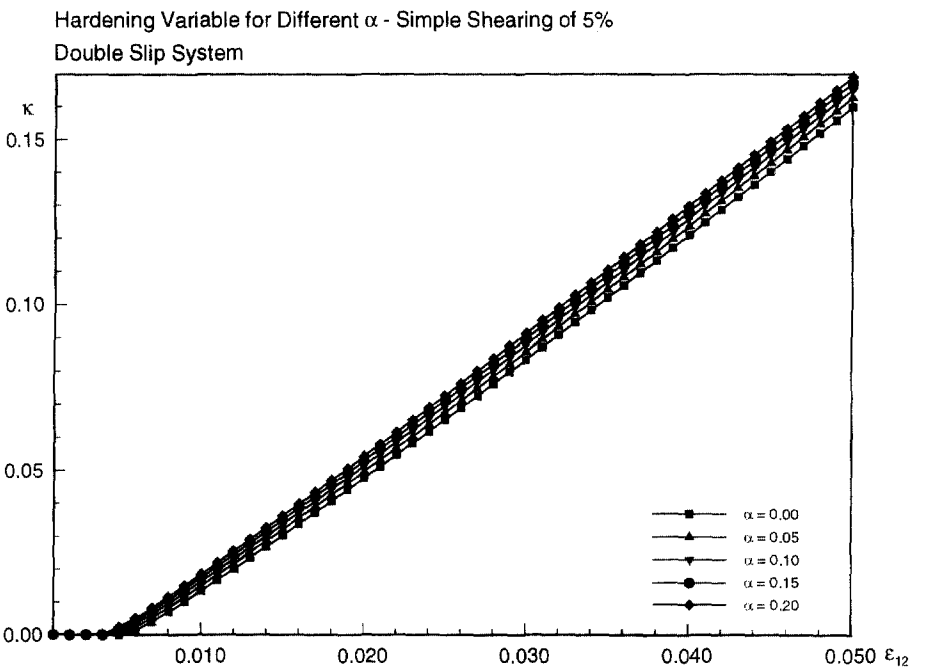

Fig. 8. Evolution of the hardening variable for different α^{min}.

somewhat earlier if non-Schmid effects are taken into account. Nevertheless, the magnitude of the different κ and Y is in the same order.

5. MULTISURFACE LOCALIZATION ANALYSIS

Classical localization analysis considers weak discontinuities, i.e. discontinuities of the strain rate field across a material surface, see e.g. Rice (1976). Analogous arguments in the

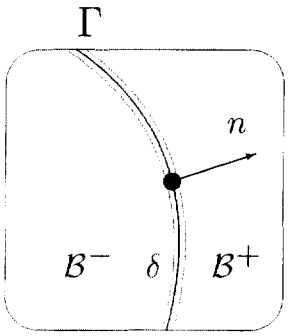

Fig. 9. Discontinuity surface.

context of planar acceleration waves in solids are found in the contributions by Hill (1962) and Mandel (1962). Recently, for single surface plasticity, the alternative kinematical concept of strong discontinuities for the description of localization has been pursued by Larsson *et al.* (1993) and Simo *et al.* (1993) for the small strain approximation and by Armero and Garikipati (1996) and Steinmann *et al.* (1997) for the geometrically nonlinear case. Localization analysis for multisurface plasticity has been considered in Steinmann (1996) and Sawischlewski *et al.* (1996).

Thereby, the condition for a regularized strong discontinuity in the displacement field $\mathbf{u}$ across a discontinuity surface Γ characterized by the surface normal $\mathbf{n}$ as depicted in Fig. 9 with jump amplitude $[\![\mathbf{u}]\!] = \mathbf{m}$ and regularization width δ is given by the localization condition

$$[[\mathscr{E}_{ep}]\!] : \dot{\boldsymbol{\varepsilon}}] \cdot \mathbf{n} + \frac{1}{\delta} \mathbf{q}_{ep} \cdot \mathbf{m} = \mathbf{0} \quad \text{with} \quad \mathbf{q}_{ep} = \mathbf{n} \cdot \mathscr{E}_{ep} \cdot \mathbf{n}. \tag{34}$$

Here, we introduced the localization tensor $\mathbf{q}_{ep}$ as the contraction of the tangent operator $\mathscr{E}_{ep}$ within the localized band with the surface unit normal $\mathbf{n}$. Thereby, the contractions are performed with respect to the second and fourth index of the fourth order tensor $\mathscr{E}_{ep}$. Taking into account the simple structure of $\mathscr{E}_{ep}$ in eqn (11) results in an intriguing concise representation of the corresponding $\mathbf{q}_{ep}$ as a sum of rank one updates of the elastic localization tensor

$$\mathbf{q}_{ep} = \mathbf{q}_{el} - \sum_{I \in \mathscr{A}} \mathbf{e}_{\mu}^{I} \otimes \tilde{\mathbf{e}}_{\nu}^{I} \quad \text{with } \mathbf{e}_{\mu}^{I} = [\mathscr{E}_{el} : \boldsymbol{\mu}_I] \cdot \mathbf{n} \quad \text{and} \quad \tilde{\mathbf{e}}_{\nu}^{I} = [\tilde{\mathbf{v}}_I : \mathscr{E}_{el}] \cdot \mathbf{n}. \tag{35}$$

Thereby, the $\mathbf{e}_{\mu}^{I}$ and $\tilde{\mathbf{e}}_{\nu}^{I}$ may be interpreted as "traction" vectors acting on the discontinuity surface and involve the flow directions $\boldsymbol{\mu}_I$ and the pseudo yield surface normals $\tilde{\mathbf{v}}_I$.

Moreover, we defined the jump in the tangent stiffness $[\![\mathscr{E}_{ep}]\!]$ in eqn (34) since $\mathscr{E}_{ep}$ might take, in general, different values inside and outside a localized band.

Next, the localization condition in eqn (34) might be considered for different loading scenarios inside and outside the localization band. Thereby, under the assumption that no discontinuity has developed so far we concentrate on the investigation of the condition for the onset of localization. On the one hand, we restrict ourselves to the basic case of continuous localization characterized by further plastic loading of all active constraints on both sides of the discontinuity and on the other hand to the limiting case of discontinuous localization where the domain outside the band completely unloads elastically whereas the domain inside the band continues to be loaded plastically for all active constraints.

5.1. *Continuous localization*

For the onset of continuous localization we consider the case of plastic loading on both sides of the discontinuity, thus the jump in the elasto-plastic tangent operator $[\![\mathscr{E}_{ep}]\!]$

vanishes identically. Upon introducing this result into eqn (34), the condition for the onset of continuous localization is then formulated as

$$\mathbf{q}_{ep} \cdot \mathbf{m} = \mathbf{0} \rightsquigarrow \det \mathbf{q}_{ep} = 0. \tag{36}$$

Observe that the regularization width δ does not come into play for this scenario and thus, remains undetermined.

Within the context of quasi-static boundary value problems, the first occurrence of the singularity of the localization tensor is referred to as the loss of ellipticity, which is synonymous with the appearance of real characteristics associated with governing equations of the hyperbolic type. Likewise, within the context of dynamic initial boundary value problems, the singularity of the localization tensor is connected with the loss of hyperbolicity.

Following the developments in Steinmann (1996) and Sawischlewski *et al.* (1996) the determinant of $\mathbf{q}_{ep}$ for a general number of independent active constraints is given in terms of the so-called ω_{IJ} matrix

$$\det \mathbf{q}_{ep} = \det \mathbf{q}_{el} \det \boldsymbol{\omega} \quad \text{with} \quad \omega_{IJ} = \delta_{IJ} - \tilde{\mathbf{e}}_v^I \cdot \mathbf{q}_{el}^{-1} \cdot \mathbf{e}_\mu^J \quad \forall I, J \in \mathscr{A}. \tag{37}$$

Therefore, since the coefficients $h_{IJ} = \eta_{IJ} + H_{IJ}$ are linearly contained in the $\tilde{\mathbf{e}}_v^I$ via the pseudo surface normals $\tilde{\mathbf{v}} = \Sigma_{J \in \mathscr{A}} h^{IJ} \mathbf{v}_J$, the critical hardening moduli H_{IJ}^{cr}, rendering $\det \mathbf{q}_{ep} = 0$, might easily be extracted from $\det \boldsymbol{\omega} = 0$. Clearly, for multiple active constraints the explicit result depends on the particular structure of the hardening moduli H_{IJ} under consideration. Typically, for isotropic hardening of all yield mechanisms with $H_{IJ} = H$ we obtain

$$H^{cr} = \max_{|\mathbf{n}|=1} \left(\left[\sum_{I,J \in \mathscr{A}} \{ \mathbf{e}_v^K \cdot \mathbf{q}_{el}^{-1} \cdot \mathbf{e}_\mu^L - \boldsymbol{\nu}_K : \mathscr{E}_{el} : \boldsymbol{\mu}_L \}^{IJ} \right]^{-1} \right). \tag{38}$$

Here we introduced the notation $\mathbf{e}_v^I = [\boldsymbol{\nu}_I : \mathscr{E}_{el}] \cdot \mathbf{n}$ and $\{(\cdot)_{KL}\}^{IJ}$ denote the coefficients with indices IJ of the inverse of a matrix with coefficients $(\cdot)_{KL}$.

Accordingly, for the special case of self-hardening of all yield mechanisms with $H_{IJ} = H\delta_{IJ}$ the critical hardening modulus follows from an eigenvalue problem as

$$H^{cr} = \max_{|\mathbf{n}|=1} \left(\max_K \lambda_K (\mathbf{e}_v^I \cdot \mathbf{q}_{el}^{-1} \cdot \mathbf{e}_\mu^J - \boldsymbol{\nu}_I : \mathscr{E}_{el} : \boldsymbol{\mu}_J) \right). \tag{39}$$

Finally, for only one active constraint these results boil down to the well-known representation

$$H^{cr} = \max_{\mathbf{n}=1} (\mathbf{e}_v \cdot \mathbf{q}_{el}^{-1} \cdot \mathbf{e}_\mu) - \boldsymbol{\nu} : \mathscr{E}_{el} : \boldsymbol{\mu}. \tag{40}$$

Interestingly, in this case ω coincides with the smallest eigenvalue of the general right eigenvalue problem $\mathbf{q}_{ep} \cdot \mathbf{z} = \omega \mathbf{q}_{el} \cdot \mathbf{z}$.

5.2. *Discontinuous localization*

Another possible loading situation within multisurface elasto-plasticity is characterized by plastic loading of all active constraints within and complete elastic unloading outside the anticipated localized band, while it is still assumed that no band has developed so far. The tangent operator within the band will then get an additional contribution due to the plastic loading condition such that we obtain the condition for onset of discontinuous localization as

$$\frac{1}{\delta}\mathbf{q}_{ep}\cdot\mathbf{m}=\sum_{I\in\mathscr{A}}\gamma_I^-\,\mathbf{e}_\mu^I. \tag{41}$$

Here, γ_I^- denote the negative "plastic multipliers", which reflect the elastic unloading condition outside the band. Accordingly, the γ_I^+ denote the positive plastic multipliers and reflect the plastic loading condition inside the band

$$\gamma_I^- = \tilde{\mathbf{v}}_I : \mathscr{E}_{el} : \dot{\boldsymbol{\varepsilon}} < 0 \quad \text{and} \quad \gamma_I^+ = \tilde{\mathbf{v}}_I : \mathscr{E}_{el} : \left[\dot{\boldsymbol{\varepsilon}} + \frac{1}{\delta}\mathbf{m}\otimes\mathbf{n}\right] > 0. \tag{42}$$

Observe that the jump amplitude δ is contained in the condition for discontinuous localization and, moreover, is indirectly driven by the continuous part of the strain rate $\dot{\boldsymbol{\varepsilon}}$. Thereby, it turns out that the solution for the jump vector $\mathbf{m}$ is given by

$$\frac{1}{\delta}\mathbf{m}=\sum_{I,J\in\mathscr{A}}\mathbf{q}_{el}^{-1}\cdot\mathbf{e}_\mu^I\,\omega^{IJ}\gamma_J^-. \tag{43}$$

Then, by checking under which condition the above localization mode complies with the assumed loading scenario we obtain the following relation between the negative γ_I^- and the positive γ_J^+ in terms of the ω_{IJ} matrix introduced in the previous section

$$\gamma_I^- = \sum_{J\in\mathscr{A}}\omega_{IJ}\gamma_J^- < 0. \tag{44}$$

Finally, the quadratic form of ω_{IJ} computed with vectors containing the γ_J^- renders a strictly negative value

$$\sum_{I\in\mathscr{A}}\gamma_I^+\gamma_I^- = \sum_{I,J\in\mathscr{A}}\gamma_I^-\omega_{IJ}\gamma_J^+ = \frac{1}{2}\sum_{I,J\in\mathscr{A}}\gamma_I^+[\omega_{IJ}+\omega_{JI}]\gamma_J^+ < 0. \tag{45}$$

Thus, as a necessary condition for discontinuous localization, at least one eigenvalue of the symmetrized ω_{IJ} matrix $\omega_{IJ}^{\mathrm{sym}}$ has to be negative. Moreover, as an additional requirement for the necessary condition for discontinuous localization to hold, all entries γ_I^- in the corresponding eigenvector have to be strictly positive and have to be mapped into strictly negative values by the original matrix ω_{IJ}. A well-known result in algebra, sometimes referred to as the Bromwich theorem, states that the eigenspectrum of a symmetrized matrix bounds the corresponding real eigenspectrum of the nonsymmetric matrix. Since ω_{IJ} is generally nonsymmetric, we therefore conclude that discontinuous localization may generally precede continuous localization which is characterized by a zero eigenvalue of the original ω_{IJ} matrix

$$\lambda_{\min}(\omega_{IJ}^{\mathrm{sym}}) \leqslant \Re(\lambda_{\min}(\omega_{IJ})). \tag{46}$$

6. EXAMPLE: PLANAR LOCALIZATION ANALYSIS

In this example the phenomenological influence of non-Schmid effects on the localization behaviour of a single crystal undergoing arbitrary homogeneous deformations under plane strain conditions which activate only a single slip system is examined. Since in the present case the elasto-plastic tangent operator does not explicitly depend on the actual stress state but is only implicitly depended on the stress state via the selection of the active slip systems, the following analysis is valid for all homogeneous deformations activating the same active set of slip systems.

Thereby, the material parameters are chosen to model an Al–Cu alloy and are set to the values of the previous example. For the kinematics of the crystal we restrict ourselves due to the above reasoning to a planar single slip model, thus the non-Schmid effects again exclusively stem from the normal stress τ_l^{nm} and the influence value α^{nm}. The single active slip plane encloses an angle of 30° with the global $\mathbf{e}_2$ direction.

The localization analysis is performed in terms of the critical hardening modulus H^{cr}, thereby we focus again on the impact of varying influence values α^{nm} representing the non-Schmid contribution. To this end, the influence value α^{nm} is increased from $\alpha^{nm} = 0\%$, representing the special case of the underlying Schmid behaviour, to $\alpha^{nm} = 20\%$, representing strong additional non-Schmid activating mechanisms for plastic slip. For a planar application the critical orientation $\mathbf{n}^{cr}$ of a possible localization band is given in terms of the in-plane angle ϑ as $\mathbf{n}^{cr} = [\cos\vartheta^{cr}, \sin\vartheta^{cr}]$.

Figures 10–14 display the hardening modulus $H = \mathbf{e}_v \cdot \mathbf{q}_{el}^{-1} \cdot \mathbf{e}_\mu - \boldsymbol{\nu} : \mathscr{E}_{el} : \boldsymbol{\mu}$ over the variation of ϑ between 0° and 360°. The maxima of these curves denote the critical values H^{cr} with the corresponding ϑ^{cr} indicating the in-plane normal to a possible localization band.

Figure 10 reflects the typical results for associated single crystal plasticity based on the Schmid law. The maximum hardening modulus $H^{cr} = 0$ is zero and corresponds to the four critical directions $\vartheta^{cr} = 60, 150, 240°$ and $\vartheta^{cr} = 330°$. Thereby, the $\vartheta^{cr} = 150°, 330°$ solutions correspond to a localization band parallel to the direction of slip **s**, whereas the $\vartheta^{cr} = 60°$, 240° solutions depict a localization band parallel to the slip plane normal **m**. For an interpretation recall that the direction $\boldsymbol{\mu}$ of the plastic strain rate $\dot{\boldsymbol{\varepsilon}}$ is given by the symmetrized dyadic product of **s** and **m**, thus, a secondary slip system with slip direction **m** and slip plane normal **s** is kinematically not distinguishable from the original one.

Figures 11–14 characterize an increasing influence of non-Schmid effects. Interestingly, in contrast to the four maxima H^{cr} in the previous Schmid case, the non-Schmid contributions emphasize roughly the slip direction **m** for the secondary slip system, resulting in only two maxima H^{cr} with corresponding critical directions $\vartheta^{cr} = 60° + \Delta\vartheta$ and $\vartheta^{cr} = 240° + \Delta\vartheta$ as depicted in the diagrams. The deviation $\Delta\vartheta$, indicating a mismatch between the secondary slip direction and the possible localization band, increases with increasing α^{nm} and is approximately 6° for the extreme case $\alpha^{nm} = 0.20\%$.

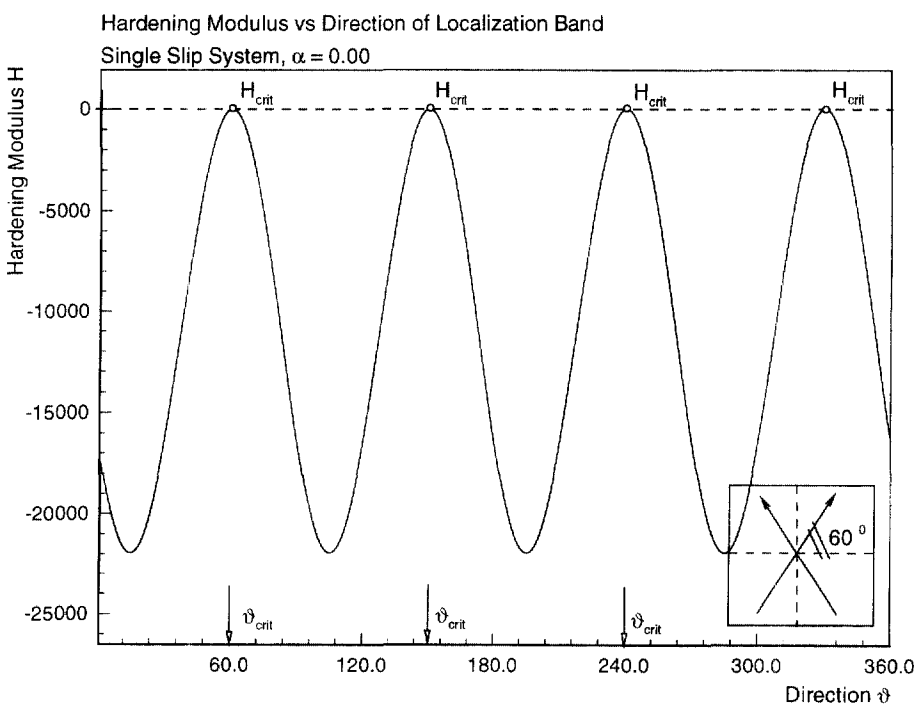

Fig. 10. Hardening modulus vs direction of localization band for $\alpha^{nm} = 0.00$.

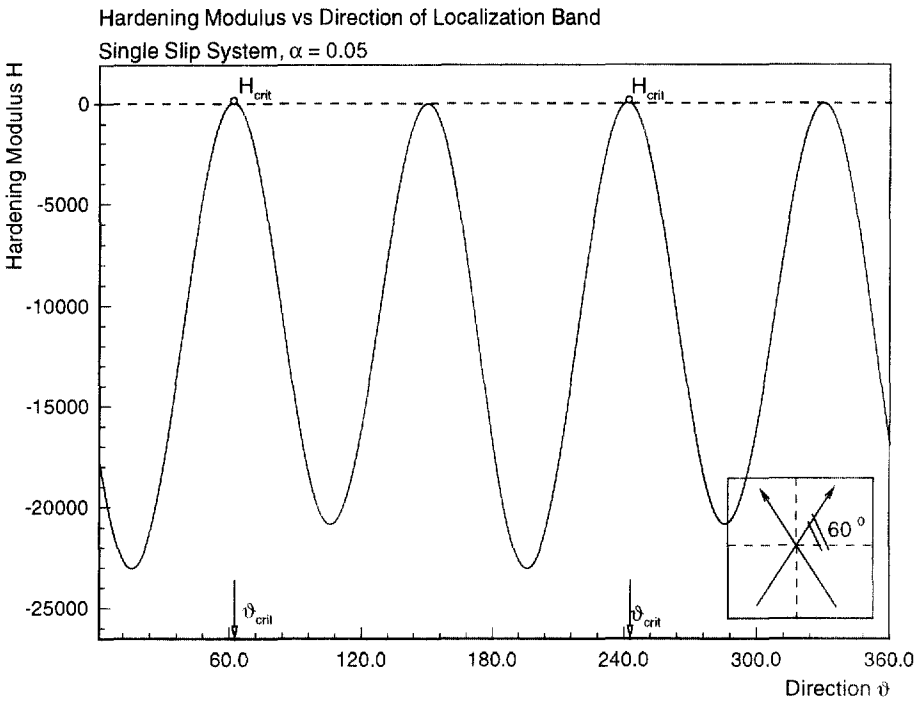

Fig. 11. Hardening modulus vs direction of localization band for $\alpha^{mm} = 0.05$.

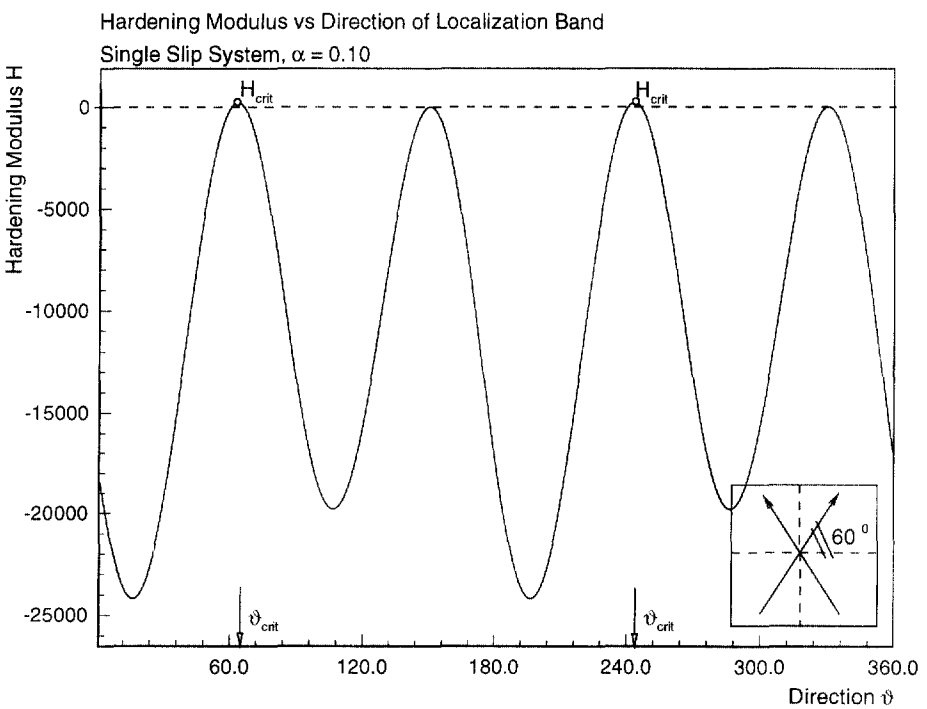

Fig. 12. Hardening modulus vs direction of localization band for $\alpha^{mm} = 0.10$.

Another important difference to the results of Schmid based single crystal plasticity stems from the non-normality of the flow rule. In contrast to Fig. 10, the critical hardening modulus now takes increasingly positive values in Figs 11–14. This is a direct consequence of the increasing non-symmetry of the tangent operator with increasing α^{mm}.

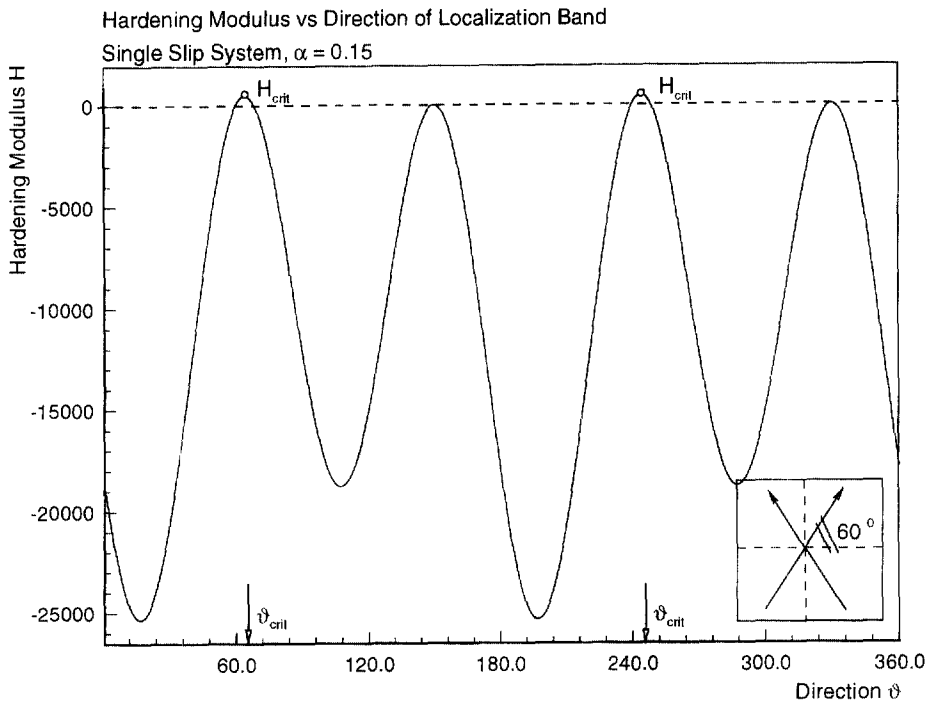

Fig. 13. Hardening modulus vs direction of localization band for $\alpha^{max} = 0.15$.

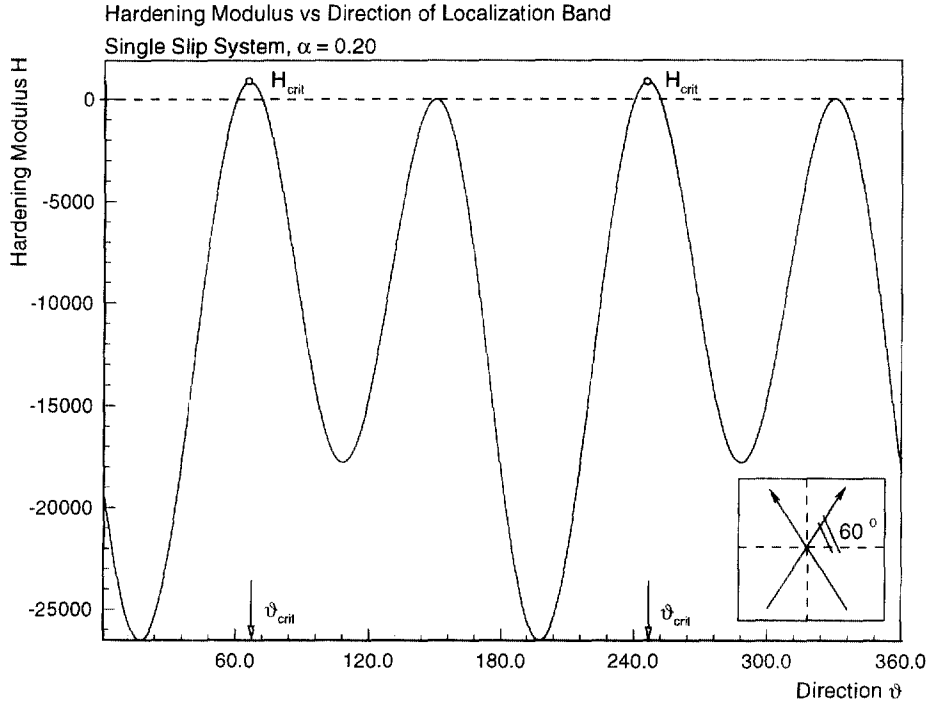

Fig. 14. Hardening modulus vs direction of localization band for $\alpha^{max} = 0.20$.

Finally, throughout Figs 11–14 we observe a zero hardening modulus H for $\vartheta^{cr} = 150^{\circ} + \Delta\vartheta$ and $\vartheta^{cr} = 330^{\circ} + \Delta\vartheta$, thus, a secondary localization band is possible as soon as the yield resistance Y has saturated with $H = 0$.

Clearly, by activating the alternative slip system with the corresponding slip plane enclosing an angle of -30° with the global $\mathbf{e}_2$ direction, the resulting curves for H are shifted by an angle of 60° with respect to the previous results.

7. SUMMARY

Motivated by the discrepancy between classical Schmid based single crystal formulations and documented experimental results, the objective of the present work has been to investigate different aspects of a single crystal plasticity formulation which takes into account additional non-Schmid effects. To this end, two non-Schmid stresses acting as additional driving forces for dislocation flow have been motivated by the crystallographic geometry. These two non-Schmid stresses, the projection onto the slip plane normal, i.e. the normal stress on the slip plane, and the projection onto the co-slip direction, i.e. the co-shear stress on the slip plane, activate dislocation flow by either obstacle jumping or obstacle surrounding. For the sake of transparency, we restricted ourselves to the geometrically linear case.

The considered single crystal plasticity formulation was recast within the continuum mechanics framework of multisurface elasto-plasticity. As a side aspect, we gave the elasto-plastic tangent operator and its inverse in a concise format of a sum of rank one updates. Based on a prototype non-Schmid single crystal model we discussed the straightforward extension of known algorithmic settings to the present non-associated case.

The influence of non-Schmid effects and non-associativity on the response behaviour of a single crystal was then investigated for the example of a simple shear deformation. Thereby, it turned out that increasing non-Schmid effects result in a decrease of the overall load carrying capacity of the sample. Moreover, the distinction between a non-associated and an associated formulation is smaller than expected. Since, from a computational point of view, an associated formulation would be preferable, this aspect deserves more attention in the future.

Subsequently, the theoretical framework for the localization analysis within multisurface plasticity was proposed. To this end, the localization conditions for continuous and discontinuous localization were derived. In particular, the possibility for several active slip systems has been taken into account and explicit results for the critical hardening modulus were given which retain the formal structure of the results obtained in the single-surface case.

Finally, the impact of non-Schmid effects on the orientation of a possible localization band and the corresponding critical hardening modulus were analysed. Thereby, we focused on the effects of the non-associated flow rule which is due to the consideration of the additional non-Schmid contributions. As a result, these additional contributions lead to destabilizing effects, thus even for positive hardening moduli the tendency towards the formation of localization bands can be predicted. Moreover, the orientation of the localization band and the active slip planes do not agree, but obey a slight mismatch angle. These two results coincide qualitatively with documented experimental observations.

In summary, this work investigated different aspects of the modelling, the computational treatment and the localization analysis of non-Schmid single crystal plasticity and highlighted the results for cases of simple model problems.

REFERENCES

Anand, L. and Kothari, M. (1996) A computational procedure for rate independent crystal plasticity. *Journal of Mechanics and Physics of Solids* **44,** 525–558.

Asaro, R. J. (1983) Crystal plasticity. *Journal of Applied Mechanics ASME* **50,** 921–934.

Asaro, R. J. (1983) Micromechanics of crystals and polycrystals. *Advances in Applied Mechanics* **23,** 1–113.

Asaro, R. J. and Rice, J. R. (1977) Strain localization in ductile single crystals. *Journal of Mechanics and Physics of Solids* **25,** 309–338.

Armero, F. and Garikipati, K. (1996) An analysis of strong discontinuities in multiplicative finite strain plasticity and their relation with the numerical simulation of strain localization in solids. *International Journal of Solids and Structures* **33,** 2863–2886.

Bassani, J. (1994) Plastic flow of crystals. *Advances in Applied Mechanics* **30,** 192–254.

Chang, Y. W. and Asaro, R. J. (1981) An experimental study of shear localization in aluminium–copper single crystals. *Acta Met.* **29,** 241–257.

Christian, J. W. (1983) Some surprising features of the plastic deformation of body-centered cubic metals and alloys. *Metall. Trans. A* **14A,** 1237–1256.

Borja, R. I. and Wren, J. R. (1993) Discrete micromechanics of elastoplastic crystals. *International Journal of Numerical Methods in Engineering* **36,** 3815–3840.

Cuitiño, A. and Ortiz, M. (1992) Computational modelling of single crystals. *Modelling Simul. Mater. Sci. Eng.* **1,** 225–263.

Ezz, S. S., Pope, D. P. and Vitek, V. (1992) Asymmetry of plastic flow in Ni_3Ga single crystals. *Acta Met.* **35,** 1879–1885.

Hill, R. (1962) Acceleration waves in solids. *Journal of Mechanics and Physics of Solids* **10,** 1–16.

Hill, R. (1966) Generalized constitutive relations for incremental deformation of metal crystals by multislip. *Journal of Mechanics and Physics of Solids* **14,** 95–102.

Hill, R. and Havner, K. S. (1982) Perspectives in the mechanics of elasto-plastic crystals. *Journal of Mechanics and Physics of Solids* **30,** 5–22.

Koiter, W. T. (1960) General theorems of elasto-plastic solids. In *Progress in Solid Mechanics*, ed. I. N. Sneddon and R. Hill. North Holland Publishing Company.

Larsson, R., Runesson, K. and Ottosen, N. S. (1993) Discontinuous displacement approximation for capturing plastic localization. *International Journal of Numerical Methods in Engineering* **36,** 2087–2105.

Leroy, F., Duranseaud, J. M. and Goux, C. (1970) Influence des contraints normales a la direction de glissement sur la valeur des cissions d'amorcage et de progression du glissement determinées par essai de traction. *Acta Metallurgica* **18,** 531–539.

Mandel, J. (1962) Ondes plastiques dans un milieu indéfini à trois dimensions. *J. Mécanique* **1,** 3–30.

Mandel, J. (1972) Plasticité classique et viscoplasticité. *Cours au CISM No.* 97, *Udine* '71. Springer, Berlin.

Miehe, C. (1996) Multisurface thermoplasticity for single crystals at large strains in terms of Eulerian vector updates. *International Journal of Solids and Structures* **33,** 3103–3130.

Paidar, V., Pope, D. P. and Vitek, V. (1984) A theory of the anomalous yield behaviour in $L1_2$ ordered alloys. *Acta Met.* **32,** 435–448.

Qin, Q. and Bassani, J. L. (1992a) Non-Schmid yield behaviour in single crystals. *Journal of Mechanics and Physics of Solids* **40,** 813–833.

Qin, Q. and Bassani, J. L. (1992b) Non-associated plastic flow in single crystals. *Journal of Mechanics and Physics of Solids* **40,** 835–862.

Rice, J. R. (1976) The localization of plastic deformation. In *Theoretical and Applied Mechanics*, ed. W. T. Koiter. North Holland, Amsterdam.

Sawischlewski, E., Steinmann, P. and Stein, E. (1996) Modelling and computation of instability phenomena in multisurface plasticity. *Comp. Mech.* **18,** 245–258.

Simo, J. C., Kennedy, J. G. and Govindjee, S. (1988) Non-smooth multisurface plasticity and viscoplasticity. Loading/unloading conditions and numerical algorithm. *International Journal of Numerical Methods in Engineering* **26,** 2161–2185.

Simo, J. C., Oliver, J. and Armero, F. (1993) An analysis of strong discontinuities induced by strain-softening in rate-independent inelastic solids. *Comp. Mech.* **12,** 277–296.

Spitzig, W. A. (1981) Deformation behavior of nitrogenated F_e–T_i–M_o and F_e–T_i single crystals. *Acta Met.* **29,** 1359–1377.

Steinmann, P. and Stein, E. (1996) On the numerical treatment and analysis of finite deformation ductile single crystal plasticity. *Comp. Meth. Appl. Mech. Engr.* **129,** 235–254.

Steinmann, P. (1996) On localization analysis in multisurface hyperelasto-plasticity. *Journal of Mechanics and Physics of Solids* **44,** 1691–1713.

Steinmann, P., Larsson, R. and Runesson, K. (1997) On the localization properties of multiplicative hyperelasto-plastic continua with strong discontinuities. *International Journal of Solids and Structures* **34,** 969–990.

Takasugi, T., Hirakawa, S., Izumi, O., Ono, S. and Watanabe, S. (1987) Plastic flow of Co_3Ti single crystals. *Acta Met.* **35,** 2015–2026.